10/1115-938-5①

SANDIA REPORT

SAND93—0172 • UC—704
Unlimited Release
Printed September 1993

Advances in Preparing and Characterizing Low Density Pan-Carbon Microcellular Foam

R. R. Lagasse, P. K. Leslie, K. R. Thompson, R. J. Weagley

Prepared by
Sandia National Laboratories
Albuquerque, New Mexico 87185 and Livermore, California 94550
for the United States Department of Energy
under Contract DE-AC04-76DP00789

SF2900Q(8-81)

DISTRIBUTION OF THIS DOCUMENT IS UNLIMITED

Issued by Sandia National Laboratories, operated for the United States Department of Energy by Sandia Corporation.

NOTICE: This report was prepared as an account of work sponsored by an agency of the United States Government. Neither the United States Government nor any agency thereof, nor any of their employees, nor any of their contractors, subcontractors, or their employees, makes any warranty, express or implied, or assumes any legal liability or responsibility for the accuracy, completeness, or usefulness of any information, apparatus, product, or process disclosed, or represents that its use would not infringe privately owned rights. Reference herein to any specific commercial product, process, or service by trade name, trademark, manufacturer, or otherwise, does not necessarily constitute or imply its endorsement, recommendation, or favoring by the United States Government, any agency thereof or any of their contractors or subcontractors. The views and opinions expressed herein do not necessarily state or reflect those of the United States Government, any agency thereof or any of their contractors.

Printed in the United States of America. This report has been reproduced directly from the best available copy.

Available to DOE and DOE contractors from
Office of Scientific and Technical Information
PO Box 62
Oak Ridge, TN 37831

Prices available from (615) 576-8401, FTS 626-8401

Available to the public from
National Technical Information Service
US Department of Commerce
5285 Port Royal Rd
Springfield, VA 22161

NTIS price codes
Printed copy: A03
Microfiche copy: A01

SAND93-0172
Unlimited Release
Printed September 1993

Distribution
Category UC-704

ADVANCES IN PREPARING AND CHARACTERIZING LOW DENSITY PAN-CARBON MICROCELLULAR FOAM

R. R. Lagasse and P. K. Leslie
Organic Materials Processing Department 1815

K. R. Thompson
NDT Technology Department 2752

R. J. Weagley
Organic Materials Synthesis and Degradation Department 1811

Sandia National Laboratories
Albuquerque, NM 87185

Abstract

This report documents an improvement in the preparation of low density microcellular carbon as well as a characterization of the spatial homogeneity of that material. In addition, the report documents in detail the process for preparing the microcellular carbon from poly(acrylonitrile) raw material. In this process, a microcellular polymer precursor (typical density = 0.025 g/cc) is first prepared via a solution-based process and then pyrolyzed to produce the microcellular carbon in a monolithic form (typical density = 0.05 g/cc). The process improvement developed in this study permits the pore structure of the microcellular polymer precursor and the microcellular carbon to be reproduced consistently in different laboratories for the first time. We determined that the pore structure is affected by an unexpected variable, the *completeness of dissolution* of the polymer raw material. That variable can be adjusted via the dissolution temperature or the particle size of the raw material. The second topic in this report involves determining the spatial fluctuation in mass density caused by periodic, millimeter-scale bands, known as "tree rings". These are clearly visible on machined surfaces of the carbon monoliths. To measure the fluctuations, we developed a very high precision, spatially resolved X-ray transmission technique. We determined that the periodic bands caused less than ±2% variation of mass density in a microcellular carbon having average density 0.041 g/cc.

MASTER

DISTRIBUTION OF THIS DOCUMENT IS UNLIMITED

Acknowledgments

D. A. Schneider and R. A. Assink performed the ^{13}C NMR analysis of the polymer and maleic anhydride solvent. They also provided a draft of their Sandia report on that work prior to formal publication. D. N. Robinson of the Martin Marietta Oak Ridge Y-12 Plant prepared some of the microcellular foam samples for the study of process variables. R. W. Vasofsky of the Y-12 Plant and L. V. Salgado contributed valuable observations regarding the preparation process. B. B. McKenzie obtained electron micrographs of the microcellular materials. A. P. Sylwester introduced us to the problems addressed in this report.

Contents

Introduction 5
Process for Preparing Low Density Microcellular PAN and Microcellular Carbon 5
Raw material characterization 5
Preparation of Microcellular PAN Precursor 7
Preparation of Microcellular Carbon 7
Controlling the Pore Structure of the Microcellular PAN Precursor 7
Background 7
Results and Discussion 9
Characterizing Density Fluctuations
Caused by Ring Structure in Microcellular Carbon 12
Background 12
Experimental 14
Results 15
Discussion 17
Conclusions 18
Controlling the Pore Structure of the Microcellular PAN Precursor 18
Characterizing Density Fluctuations
Caused by Ring Structure in Microcellular Carbon 18
References 18

ADVANCES IN PREPARING AND CHARACTERIZING LOW DENSITY PAN-CARBON MICROCELLULAR FOAM

Introduction

Development of a process for preparing low density microcellular carbon from poly(acrylonitrile) (PAN) was initiated in the mid 1980's by C. Arnold, J. Aubert , P. Rand, and A. Sylwester(1-3). The first step in the process is to cause a phase separation of the polymer from solution by a thermal quench. The quench also causes the solvent, maleic anhydride, to crystallize. The crystallized solvent is then removed via vacuum subiimation, leaving a microcellular PAN monolith having density typically near 0.025 g/cc. Finally, the microcellular PAN is thermally pyrolyzed to produce a microcellular carbon monolith having density typically near 0.05 g/cc. The pore structure of the PAN precursor, that is, the density, void fraction, and pore size can be modified by changing certain variables in the solution quenching. Since the pore structure of the PAN precursor is closely duplicated in the final carbon, the carbon pore structure can be tailored for optimum performance in selected applications. Examples of unclassified applications for this tailored microcellular carbon are electrodes for electrochemical devices, adsorbents for purifying and storing gasses, and thermally stable supports for catalysts.

This report addresses two issues that have limited the utility of the microcellular carbon technology for certain applications (14). First, we identified an important, but previously unrecognized variable in the process for preparing the microcellular PAN precursor. This variable had been causing unacceptable variability in its pore structure and mechanical strength. Second, we characterized a peculiar defect consisting of regularly spaced bands, known as "tree rings", visible on machined surfaces of the microcellular carbon. We determined that the bands had little effect on the spatial homogeneity of the material, because they caused less than ±2% variation in mass density. In addition, this report documents the process and the analysis of raw materials used to prepare the microcellular carbon. This documentation will facilitate preparation of the novel carbon material in the future.

Process for Preparing Low Density Microcellular PAN and Microcellular Carbon

Raw material characterization

The poly(acrylonitrile) was purchased from Aldrich Chemical Company (Catalog # 18,131-5) and was used without further purification. It was determined to be an *atactic homopolymer* by ^{13}C NMR analysis (4,5). The atactic nature of the PAN homopolymer means that the nitrile side groups attached to the main chain are placed randomly on either side of the chain. The ^{13}C NMR spectrum shown in Fig. 1 reveals three major peaks corresponding to the three different bonding structures of carbon in the PAN repeat unit. The random tacticity of the PAN was determined by analyzing the splitting of the peak near 27 ppm. Gel permeation chromatography(5) on the PAN

yielded a poly(styrene) equivalent weight average molecular weight $M_W=7x10^5$ and a

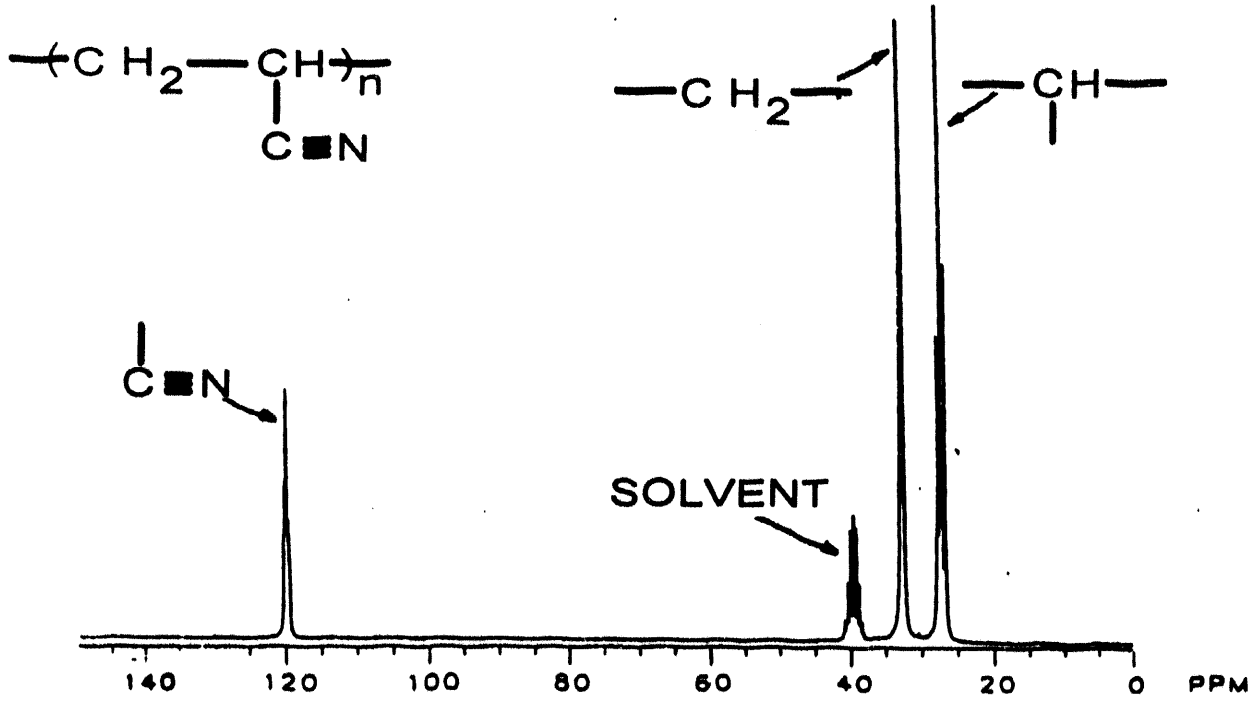

Figure 1. High resolution (50 MHz) ^{13}C NMR spectrum of PAN raw material. Assignment of the peaks to the various carbon atoms within the repeat unit of the polymer are shown. Splitting of the peak near 27 ppm, perhaps not apparent in the figure, was used to determine that the polymer had an *atactic* (random) placement of the nitrile side group. (Ref. 4.)

polydispersity ratio $M_W/M_n= 3$. The polydispersity of 3 is expected for a polymer prepared by free radical polymerization. Since that polymerization method is used to prepare atactic PAN(6), the measured polydispersity is consistent with the determination of an atactic chain structure by ^{13}C NMR. The GPC results are shown later in this report.

It should be noted that the PAN used in our process is different from the polymer used commercially to prepare acrylic fibers for textile applications and precursors for preparation of high strength carbon fibers. The polymers used in the commercial processes are actually *copolymers* of acrylonitrile containing a small fraction of comonomers such as vinyl acetate or itaconic acid.

The maleic anhydride solvent used for processing the PAN into a microcellular material was purchased from Monsanto Chemical Company. ^{13}C NMR spectra showed that it contained maleic acid as an impurity(4). Maleic acid is expected to be present since it is the product from reaction of maleic anhydride with atmospheric moisture. The maleic anhydride was purified via vacuum sublimation at a temperature of 30-40°C. ^{13}C NMR measurements(4) showed that the purification caused the maleic acid concentration to be reduced to 0.06 wt%.

Preparation of Microcellular PAN Precursor

The first step in processing the PAN raw material into a microcellular foam is to dissolve 1.7 wt% of the polymer in maleic anhydride at about 160°C in an evacuated and sealed flask. The vacuum, (produced by a mechanical pump) minimizes bubbles in the agitated solution, which would produce large voids in the microcellular PAN monolith. After the solution appears to be homogeneous (see discussion below), the flask is cooled to 140°C. Then the solution is poured into a heated rectangular mold. The bottom of the mold is a copper or aluminum sheet that is coated with a protective layer (approximately 3 mm) of silicone rubber. The walls of the mold are constructed of 1 inch thick silicone rubber and the opening to the mold is sealed with a silicone slab of similar thickness. The next step in the process is to cool the bottom of the mold on a water cooled copper plate held at 26°C. The mold design ensures that the cooling is primarily one dimensional, through the bottom. Since the solution is cooled below the equilibrium melting temperature of maleic anhydride (53°C), crystallization occurs. The crystallized solvent is removed from the rectangular casting by sublimation under vacuum at 30-40°C. The final rectangular monolith of microcellular PAN has a typical density of 0.025 g/cc. The density can be adjusted by varying the concentration of PAN in the original solution.

Preparation of Microcellular Carbon

The microcellular PAN is thermally pyrolyzed into microcellular carbon having similar pore structure. The pyrolysis is performed in two steps. First, the PAN monolith is heated in air using a forced convection oven. The oven temperature is increased over a period of 2 hours to 220°C and then held there for 16 hours before cooling back to ambient temperature. The second step in the pyrolysis is performed in a flowing argon atmosphere using a quartz tube furnace. The furnace temperature is raised at 4°C/min to 1000°C, held there for 1 hr, then raised at 3°C/min to 1100°C, and held there for 8 hr, before cooling back to ambient temperature. Figure 2 shows typical pore structures of the microcellular PAN and carbon. In both materials the pore size is about 3-5 μm, and the walls of the pores are made up of interconnected flakes. The similarity in pore structure means that the microcellular carbon can be tailored by adjusting the pore structure of the PAN precursor.

Controlling the Pore Structure of the Microcellular PAN Precursor

Background

Although conceptually simple, the process for preparing the PAN precursor proved to be difficult to control(7,14) Specifically, separate teams working in different laboratories had difficulty producing microcellular PAN having the same pore structure, even though they used exactly the same raw materials and they duplicated all process conditions as closely as possible. Two limiting types of pore structure were commonly observed. In one type the pores were defined by interconnected flakes, while in the other the pores were defined by spherical structures, as shown in Fig. 3. The mechanical strength of the two microcellular PAN materials shown in Fig. 3 was

dramatically different even though they had the same density, 0.025 g/cc. The material with the interconnected flake structure (Fig. 3a) was strong enough to be handled easily, and it produced a microcellular carbon that could be machined into complex shapes. In contrast, the material having the sphere structure (Fig. 3b) would invariably be damaged by handling, and it produced microcellular carbon that was too weak to machine. Another measure of the difference in mechanical properties between the two types of microcellular PAN is the Shore 000 hardness measured with a 1/2 inch spherical indenter. The PAN sample having the flake structure had a Shore hardness of 85, while the sample having the sphere structure had a hardness of 35.

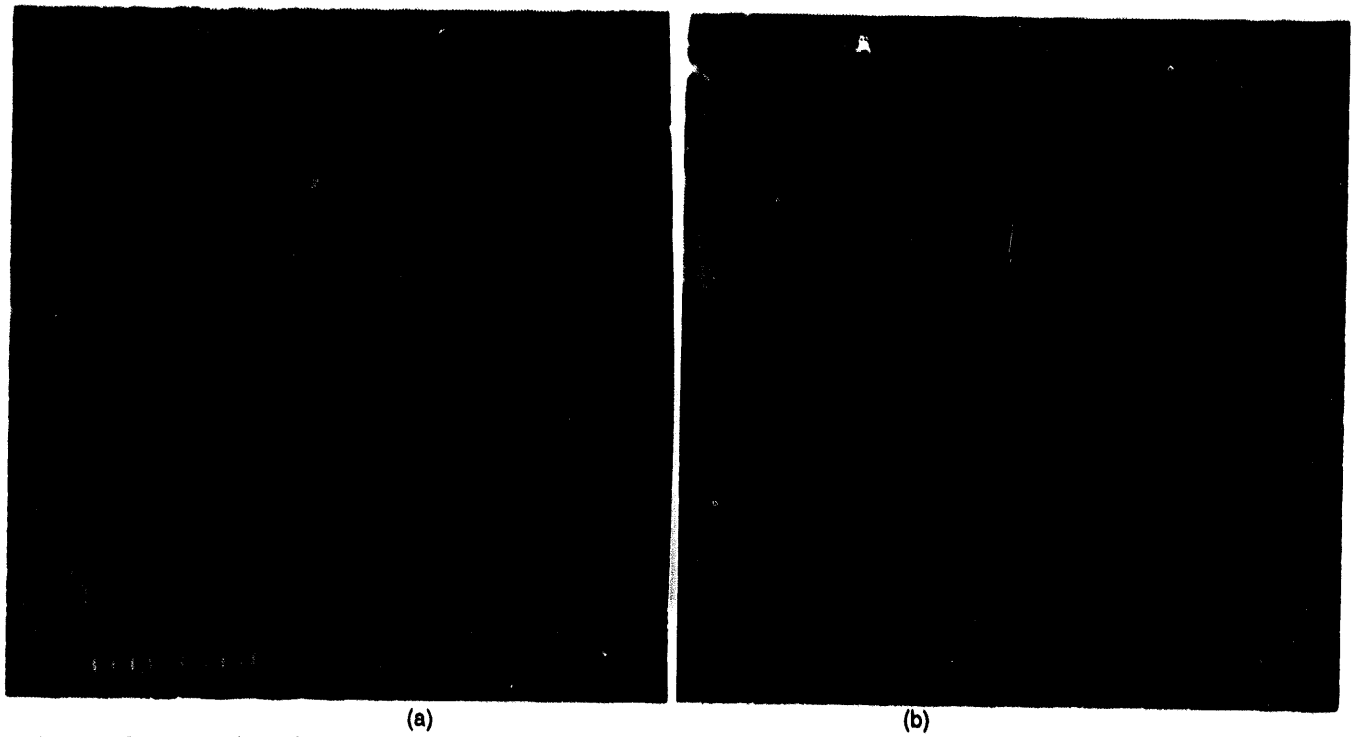

(a) (b)

Figure 2. Scanning electron micrographs (taken at the same magnification) of the microcellular PAN precursor (a) and the microcellular carbon (b) prepared from that precursor. The shape and size of the pores are very similar in the two materials. The magnification is indicated by the 5μm and 10μm white bars at the bottom of micrographs (a) and (b), respectively.

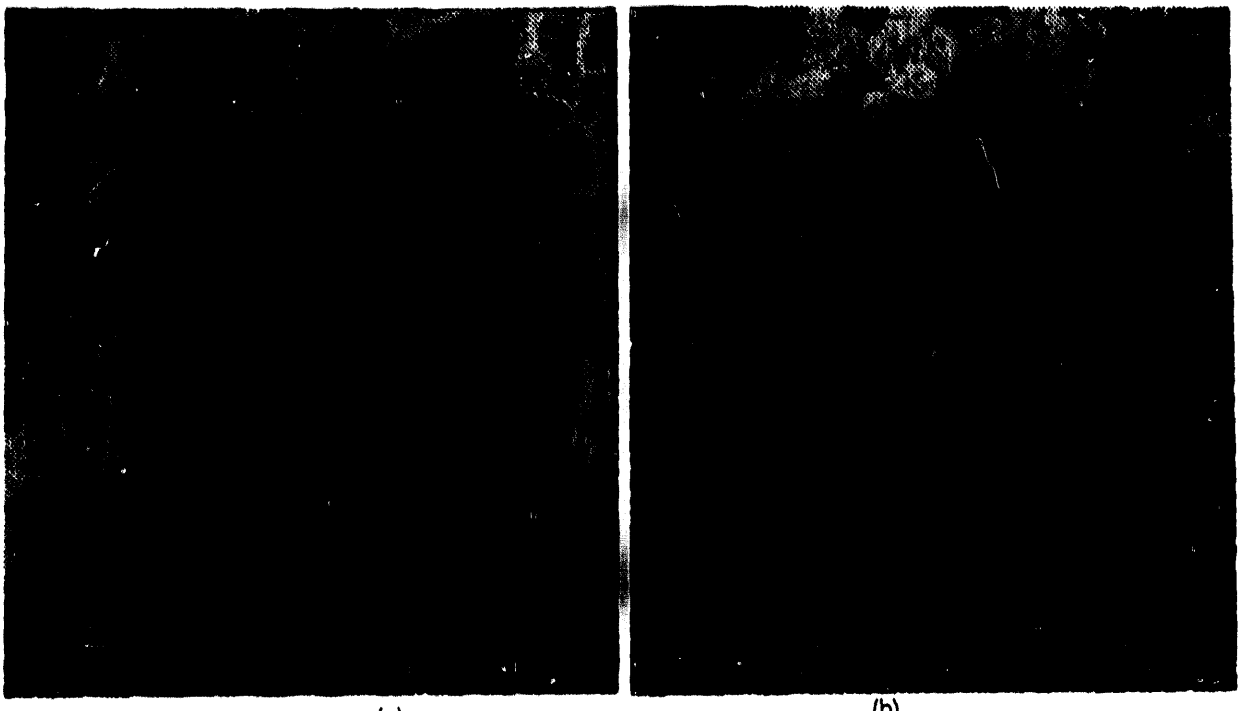

(a) (b)

Figure 3. Scanning electron micrographs of two limiting morphologies observed commonly in the microcellular PAN. In (a) the flake-like pore walls are well interconnected and the mechanical strength is higher. In (b) the flakes appear aggregated into spherical structures, reducing the degree of three dimensional interconnection. The sphere morphology produces much lower mechanical strength. The magnification is indicated by the 10μm white bar at the bottom of each photo.

Results and Discussion

A series of carefully controlled experiments showed that a very subtle difference in the method used to dissolve the PAN raw material in the maleic anhydride solvent caused the variation in pore structure and mechanical strength. First, we demonstrated that a small variation in dissolution temperature caused a significant change in pore structure and strength. We performed experiments where all composition and process variables were kept strictly constant, except for the temperature used to dissolve the PAN. When the dissolution temperature was 155°C, the final microcellular PAN had the highly interconnected flake morphology (Fig. 4a) and robust mechanical strength, indicated by a Shore hardness of 84. When the experiments were repeated with 10°C higher temperature, the morphology was less well interconnected and included larger pores (Fig. 4b), and the Shore hardness, 70, was considerably lower. The visual appearance of the PAN solutions differed markedly in the two experiments. The solution prepared at the lower temperature had a hazy appearance, indicating substantial concentration fluctuations. (No individual, undissolved particles could be resolved by visual examination, however.) In contrast, the solution prepared at the higher temperature was much clearer, indicating smaller concentration fluctuations.

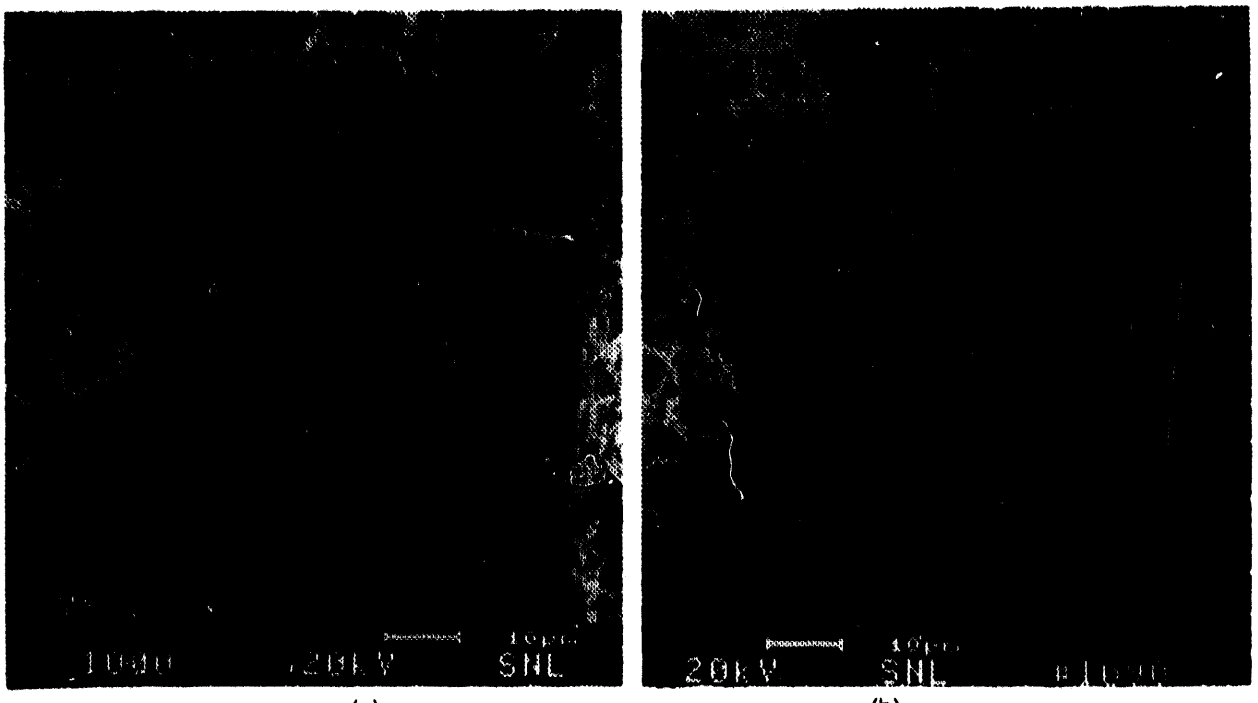

(a) (b)

Figure 4 Scanning electron micrographs of microcellular PAN materials prepared using two different temperatures for dissolving the polymer into the solvent. In (a) the dissolution temperature was 155°C and the flake-like pore walls are relatively well interconnected. In (b) the dissolution temperature was somewhat higher, 165°C, and the flakes are less well interconnected. In the latter micrograph, larger pores are visible in addition to the small pores defined by the flakes. The higher dissolution temperature produced a microcellular material having lower hardness. The magnification is indicated by the 10μm white bar at the bottom of each photo.

Although the microcellular PAN produced using the higher dissolution temperature (Fig. 4b) did not exhibit the extreme case of the sphere morphology, these experiments showed that the dissolution temperature definitely affected the pore structure and mechanical strength of the microcellular PAN. We speculate that the spherical morphology would have been produced in the experiment having higher dissolution temperature if the solution had been held at that temperature for a longer time. That speculation is based on additional experiments performed in our laboratory.

We initially hypothesized that a difference in thermal degradation of the PAN during dissolution caused the difference in the final microcellular material. This hypothesis was not supported by characterization experiments that compared the two limiting types of microcellular PAN. We first compared material having the flake structure (Fig. 3a) with material having the sphere structure (Fig. 3b) using gel permeation chromatography (GPC). Both the weight and number average molecular weights (polystyrene equivalent) measured by GPC were identical within experimental error for the two materials. Moreover, the average molecular weights for the two microcellular materials were statistically identical to those of the PAN raw material. The chromatograms used to derive the average molecular weights are shown in Fig. 5. The chromatograms represent a separation of polymer species according to their molecular weight. The abscissa represents the variation in molecular weight (increasing retention time corresponding to decreasing polymer molecular weight) and the ordinate is proportional to the concentration of each species. The

chromatograms do not reveal any difference in the distribution of molecular weights between the

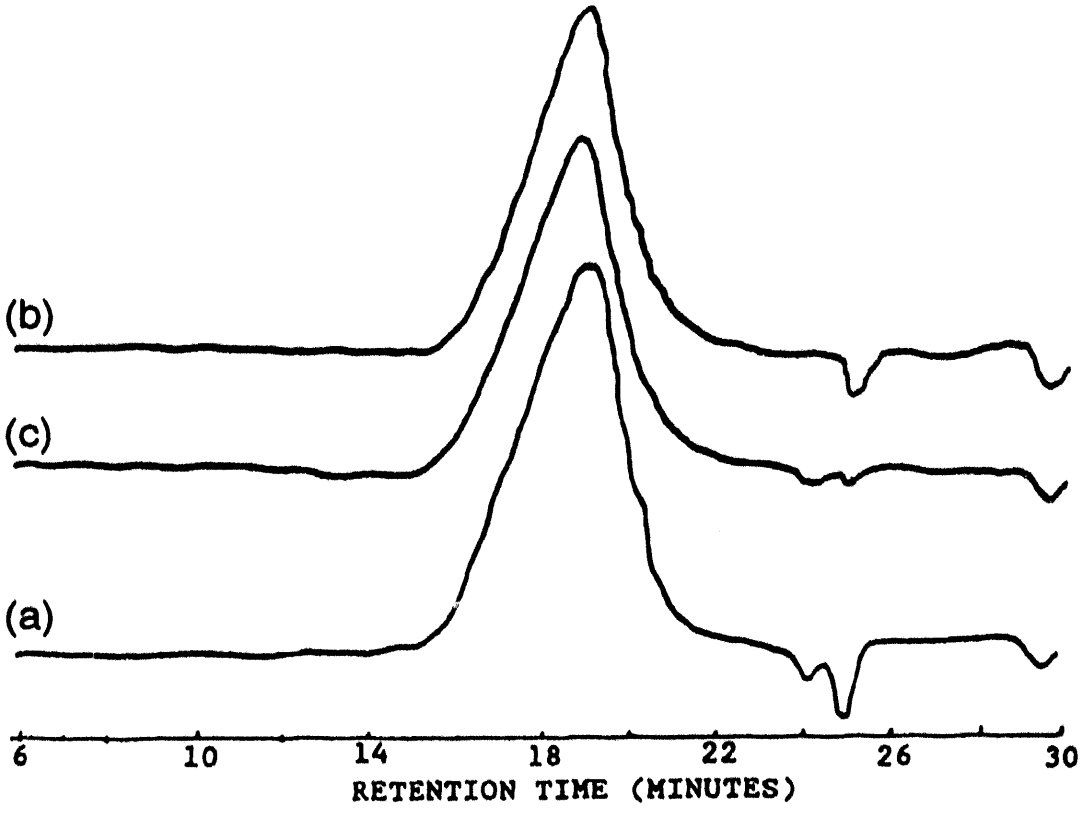

Figure 5. Gel permeation chromatograms comparing the distribution of molecular weights in the PAN raw material (a), the mechanically weaker microcellular PAN having the sphere-type pore structure (b), and the mechanically stronger microcellular PAN having the flake-type pore structure (c).

two microcellular materials and the PAN raw material.

Two other characterization techniques, infrared spectroscopy and NMR spectroscopy, also revealed no difference in the molecular structure between the two limiting microcellular materials. Fourier transform infrared spectra are sensitive to asymmetric modes of vibration between the atoms of the PAN molecule. The close similarity in infrared spectra (Fig. 6) between the two limiting microcellular materials means that no difference in molecular structure could be detected by this technique. ^{13}C NMR spectra on the two microcellular materials were identical to each other and indistinguishable from the spectrum of the PAN raw material (Fig. 1). In summary, neither gel permeation chromatography, infrared spectroscopy, nor ^{13}C NMR spectroscopy revealed any evidence for a variation in the degree of degradation in PAN molecular structure during dissolution at elevated temperatures that could explain the difference in pore structure and mechanical strength of the two microcellular materials.

A final experiment added independent evidence that degradation in molecular structure did not cause the difference in the microcellular materials. Here we produced the two limiting pore

structures by simply *varying the particle size of the PAN raw material* used to prepare the solution, while *keeping all other variables, including the dissolution temperature constant.* A solution made with finely powdered PAN dissolved completely to a clear solution at 162°C and produced the weak sphere morphology. A solution prepared at the same temperature using PAN having a larger average particle size produced a monolith having the strong flake morphology. The morphology and strength of the latter were different even though a) the solution was filtered to remove large undissolved PAN particles and b) the concentration of PAN in the filtered solution was the same as that in the clear solution made using the fine powdered PAN. Since the dissolution temperature was the same in both cases, the extent of degradation of the polymer should also have been the same. Differences in extent of degradation, therefore, do not appear to cause the difference in pore structure. We speculate, instead, that the change in particle size of the polymer raw material at constant dissolution temperature or the change in dissolution temperature at constant particle size causes a difference in the *supermolecular structure* (larger than molecular dimensions) of the PAN macromolecules in solution. For example, variations in the completeness of dissolution of the PAN could affect the degree of aggregation of individual PAN molecules in solution. Consistent with this speculation is the fact that the PAN molecule contains nitrile side groups that are known to attract each other strongly via dipolar forces(8). Moreover, coupling of individual PAN molecules into larger aggregates in solution has been reported frequently in the literature(9-12). Further details on the work reported in this section can be found in Ref. 5.

Finally, it should be noted that more extensive studies(13) on microcellular PAN prepared using completely different process conditions have shown that raising the dissolution temperature again causes a change from the interconnected flake microstructure to the sphere microstructure similar to that shown in Fig. 3. In this case, the microcellular PAN had higher density (0.1 g/cc) and it was prepared from a more concentrated solution (10 g PAN/100 cc) using a completely different solvent (a mixture of dimethyl-formamide and ethylene glycol.) The sensitivity of pore structure to the dissolution process therefore appears to be a general phenomenon for microcellular PAN prepared using different concentrations and solvents.

Characterizing Density Fluctuations Caused by Ring Structure in Microcellular Carbon

Background

The problem addressed in this section is illustrated in a photograph of a machined surface of the microcellular carbon (Fig. 7). This shows parallel bands having a spacing of 3 mm. The bands were visible on all exterior surfaces of the specimen. Examination of surfaces exposed by machining the porous carbon revealed that the bands are present throughout the material. Examination of larger specimens revealed that the bands in Fig. 7 are actually segments of concentric rings. The distinct rings raised serious questions about the spatial homogeneity of the microcellular carbon. Homogeneity was a critical requirement for an important application (14). The objective of this portion of our work was to characterize the spatial fluctuation in mass density caused by the rings.

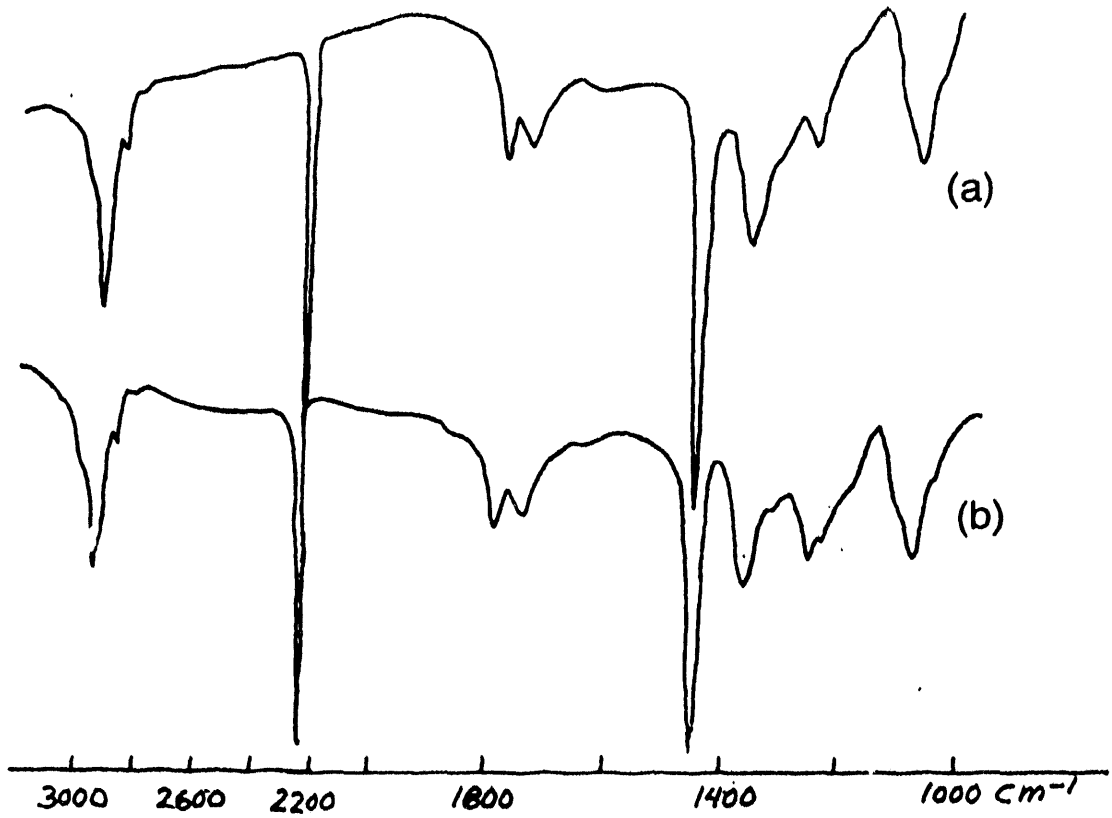

Figure 6. Fourier transform infrared spectra comparing the weaker microcellular PAN (a) with the stronger microcellular PAN (b).

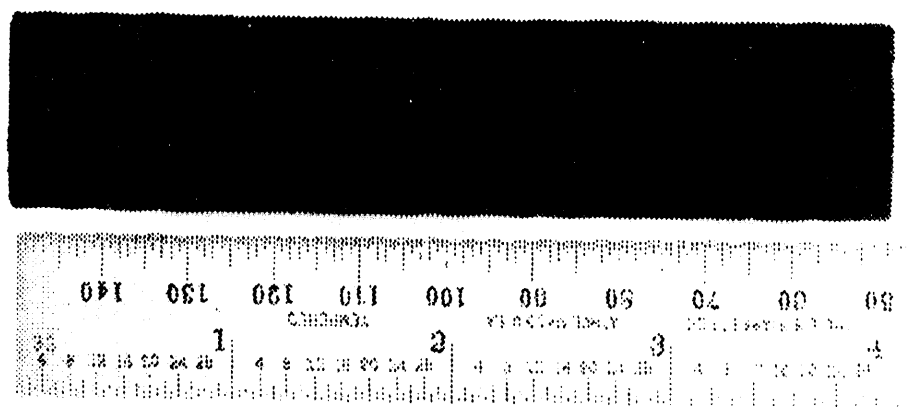

Figure 7. Photograph of a machined surface of the microcellular carbon derived from a PAN precursor. The parallel bands (known as "tree rings") visible on the surface raised serious questions about spatial fluctuations in the mass density of the porous carbon. The spatial period of the bands was typically 3-4 mm.

The density fluctuation was characterized by spatially resolved measurements of the fractional transmission of a monochromatic X-ray beam. The basis for the method will now be explained(15). When a monochromatic beam of X-rays is attenuated by absorption only (not scattering) then the fractional transmission is given by

$$\frac{I_t}{I_0} = \exp(-\mu_L t), \tag{1}$$

where I_0 is the intensity of the beam incident on the sample, I_t the intensity transmitted through the sample, μ_L the linear absorption coefficient, and t the thickness. The linear absorption coefficient for a material having mass density ρ is determined from the mass absorption coefficient for each constituent element, $(\mu_M)_i$, and the weight fraction of that element, w_i, as shown in Eq. 2.

$$\mu_L = \rho \sum_i (\mu_M)_i * w_i \tag{2}$$

(The mass absorption coefficient is simply the fractional attenuation caused by 1 gram of an element, independent of its concentration within the material.) Making the reasonable assumption that the elemental composition within the microcellular carbon is independent of spatial position means that the summation in Eq. 3 is a constant K. Then the local value of the linear absorption coefficient becomes directly proportional to the density.

$$\mu_L = \rho * K \tag{3}$$

Substituting Eq. 3 into Eq. 1 and taking the logarithm yields

$$-\ln(\frac{I_t}{I_0}) = (Kt) * \rho \tag{4}$$

Eq. 4 shows that if the thickness of the specimen is constant, the logarithm of the fractional transmission is directly proportional to the local value of the density. The percentage variation in density will then be equal to the percentage variation in the log of the fractional transmission.

Experimental

The method described above is obviously applicable to radiation sources other than X-rays. We chose to perform the measurements with X-rays because an apparatus for performing these kinds of experiments had already been built by W. D. Drotning(16). It consists of an ^{55}Fe source of X-rays (5.9 keV, wavelength=2.1 Ang. Units), a collimation system to define the size of the beam, a detector to sense the transmitted intensity, and an automated translation stage to move the beam to different positions on the specimen.

To measure small density fluctuations with millimeter spatial resolution, the collimation system in Drotning's apparatus, as well as the data acquisition system were modified substantially. Very fine collimation of the X-ray beam reduced its incident intensity. Accumulation of a large number of detector counts was necessary to achieve high precision in the measured fractional transmission in order to detect small variations in material density. Accumulating the necessary detector counts therefore required a very long measurement time at each location. A typical set of transmission measurements employed displacement increments of 0.5 mm and covered a total displacement of 15 mm over the surface of the specimen. Several days of continuous operation were required to complete the measurements on one specimen. Employing a long half-life radioisotope as an X-ray

source, instead of a conventional X-ray generator, eliminated any concern with drift in the incident X-ray intensity during the long experiments.

Results

A benchmark experiment demonstrated that the modified apparatus could detect density fluctuations on a scale of 1 mm. An array of four parallel 0.7 mm diameter metal wires having an empty space of 0.7 mm between each wire was set up as a trial specimen. Fig. 8 shows the detector output as a function of spatial position along with the ideal response expected if the wires were completely opaque across their full width. Although the results in Fig. 8 were not analyzed quantitatively, the substantial agreement between the detector output and the ideal response gave us confidence that our apparatus and technique were capable of measuring density fluctuations caused by the rings. It should be noted that the benchmark experiment was an excessively severe test of our apparatus, since the wire diameter and spacing were much smaller (four times smaller) than the spacing of the rings in the carbon material.

To determine the fluctuation in mass density caused by the rings in the microcellular carbon, we selected a specimen having rings that were favorably oriented with respect to the specimen basal

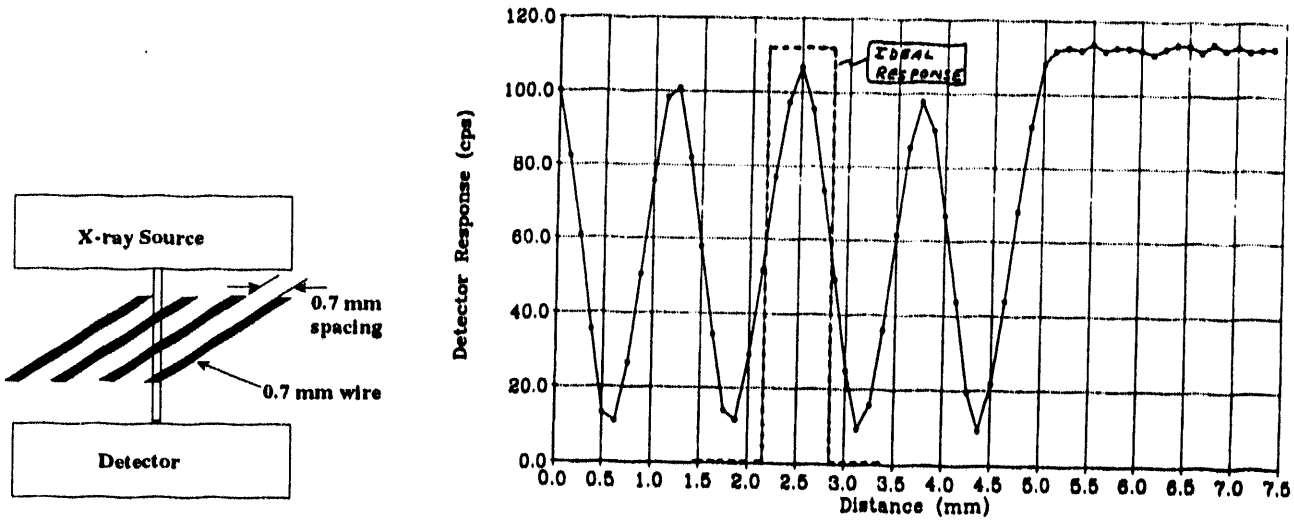

(a) (b)

Figure 8. Benchmark experiment designed to demonstrate that a high resolution X-ray transmission technique could detect density fluctuations on a length scale of 1 mm. The test sample shown in (a) consisted of four parallel 0.7 mm diameter wires with 0.7 mm spacing. The response of the X-ray intensity detector as a function of position is shown in (b). The dashed line shows the ideal response of the detector if the wires were completely opaque.

plane. That is, the rings, when viewed on the edge of the specimen were normal to its basal plane. Therefore, an X-ray beam incident normal to the basal plane should have probed a constant

structure as it propagated through the specimen thickness, as shown in Fig. 9a. Then we could determine the variation in the fractional transmission, and therefore the spatial variation in density, caused by the ring structure by translating the beam to a different location. The specimen of microcellular carbon was produced at the Martin Marietta Oak Ridge Y-12 Plant, where it was given an identification number of 1495. It was 8 mm thick, and had an average density of 41 mg/cc.

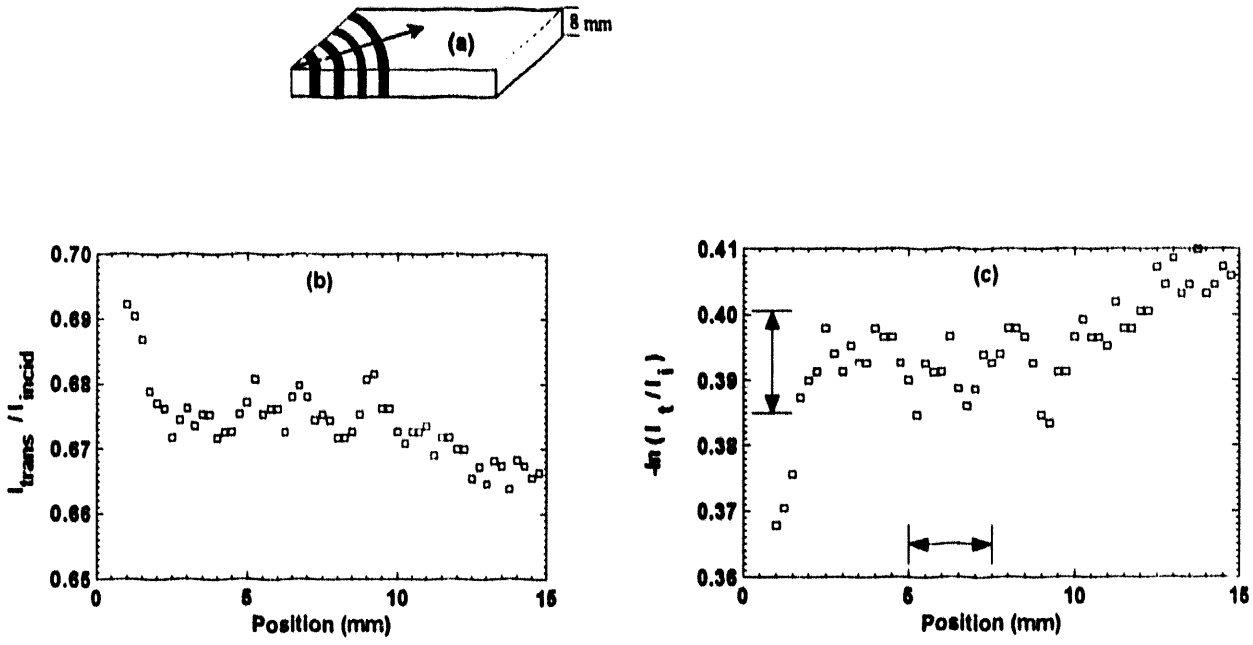

Figure 9. Results of X-ray transmission measurements along a 15 mm line on the surface of a microcellular carbon sample (a). The line follows the radial coordinate of the circular bands. The fractional transmission (b) and the natural log of the fractional transmission (c) are plotted vs. spatial position. The natural log of the fractional transmission is proportional to the local mass density of the material, according to Eq. 4. The arrow on the x-axis corresponds to the repeat distance of the rings determined visually. The arrow on the y-axis corresponds to a fluctuation in density of ± 2%.

The results of a series of transmission measurements covering 15 mm across the surface of the specimen are shown in Fig. 9. Most of the fractional transmission values ranged from 67 to 68% (Fig. 9b). At the beginning of the scan (near the corner), however, the transmission was higher because we believe that the specimen was slightly thinner there. As suggested by Eq. 4, the logarithm of the fractional transmission is plotted vs. spatial position in Fig. 9c. These results indicate that the spatial fluctuation in density has an amplitude less than ±2%. There is no clear correlation between the spatial period of the density fluctuation and the spacing of the visible rings.

The results of a second 15 mm scan along a different direction on the same specimen is shown in Fig. 10. This scan again began at a corner but proceeded along one edge of the specimen, which was oriented at an angle to the radial coordinate of the rings. The spacing between the visible bands along the displacement direction was therefore larger for this scan as compared to the previous scan. The logarithmic plot shown in Fig. 10c again shows a density fluctuation having an amplitude less than ±2% and having a spatial period unrelated to the spacing between the

visible bands.

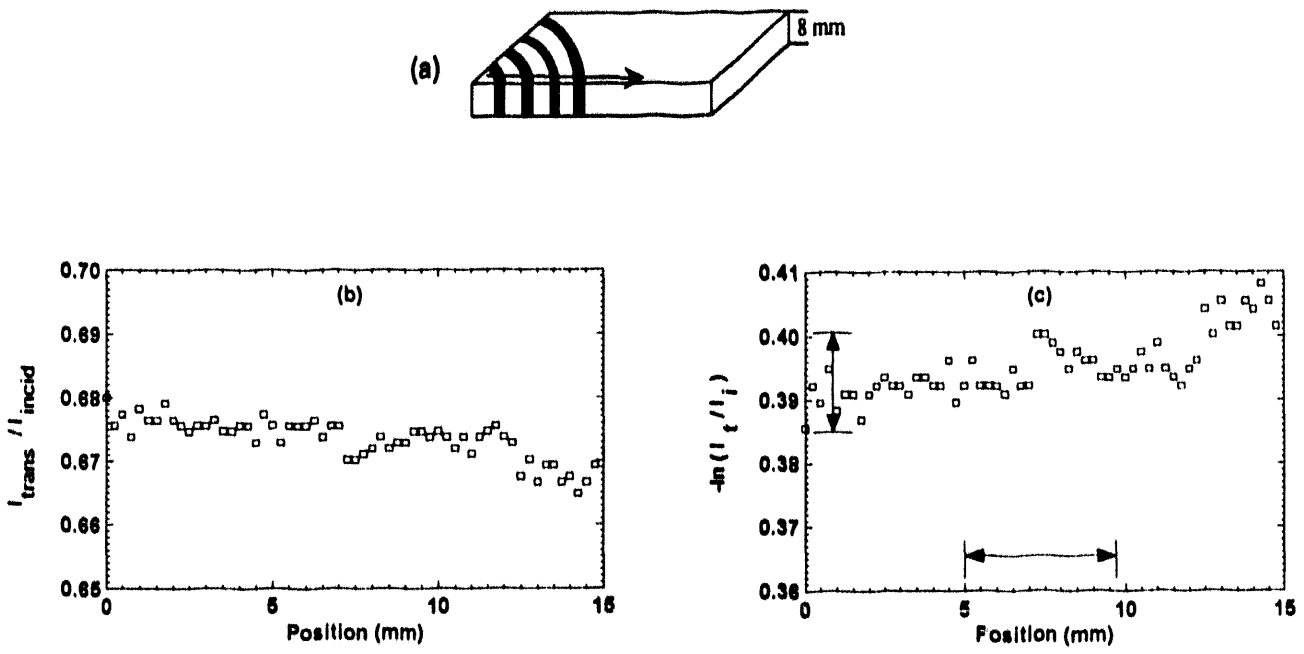

Figure 10. Results of X-ray transmission measurements along a 15 mm line inclined at an angle to the radial coordinate of the circular bands (a). The fractional transmission (b) and the natural log of the fractional transmission (c) are plotted vs. spatial position. The arrow on the x-axis corresponds to the repeat distance of the rings determined visually. The arrow on the y-axis corresponds to a fluctuation of in density of ± 2%.

Discussion

We conclude that even though concentric bands are clearly visible on machined surfaces of the microcellular carbon, they cause a fluctuation in mass density of no more than about ±2%. In fact, we believe that the small spatial variation in the fractional transmission of X-rays may be caused not by density fluctuations but by spatial fluctuations in pore size within the microcellular carbon. This speculation is based on small angle X-ray scattering (SAXS) measurements(17). The intensity of *scattered X-rays* showed a spatial fluctuation that was very clearly correlated with the visible bands. We therefore believe that our assumption of negligible attenuation due to scattering may be an oversimplification, and that some of the spatial variation seen in Fig. 9 and 10 is caused by variations in scattering instead of absorption of X-rays. We are confident, nevertheless, that our estimate of ±2% at least puts an upper limit on the spatial fluctuation in mass density caused by the ring structure.

A final topic concerns the physical mechanism that actually produces the concentric bands. This has been traced to the process used to prepare the PAN precursor for the microcellular carbon. Structural characterization during crystallization of the maleic anhydride solvent in the PAN solution has shown that the crystallization produces a spatially periodic fluctuation in the orientation of the maleic anhydride crystals. Interestingly, this periodic fluctuation in the solvent

crystal orientation remains imposed on the microcellular PAN even after the solvent is removed by sublimation. The periodic structure in the PAN precursor becomes clearly visible after the precursor is thermally pyrolyzed to produce the microcellular carbon. A detailed description of this study is outside the scope of the present report but is being documented in a separate publication(18). A brief summary has been included here to indicate our level of understanding of the peculiar ring structure in the microcellular carbon.

Conclusions

Controlling the Pore Structure of the Microcellular PAN Precursor

1. Varying the completeness of the dissolution of the poly(acrylonitrile) in maleic anhydride causes a variation in the microcellular polymer morphology and mechanical strength. The completeness of dissolution can be varied by changing the dissolution temperature or the particle size of the PAN raw material.

2. Characterization experiments sensitive to the average molecular weight and chemical structure of the poly(acrylonitrile) molecules do not reveal any difference between the strong and weak microcellular materials. We *speculate* that increasing the completeness of dissolution does not cause degradation of the PAN molecules but instead changes the conformation of the molecules in solution, e.g. the degree of aggregation of the molecules.

Characterizing Density Fluctuations Caused by Ring Structure in Microcellular Carbon

X-ray transmission measurements show that the spatial variation in mass density caused by the rings is no more than ±2% in microcellular carbon #1495 having average density 41 mg/cc.

References

1. Memorandum, C. Arnold, J. H. Aubert, P. B. Rand, R. L. Clough, and J. G. Curro to Distribution, July 8, 1985.

2. A. P. Sylwester, J. H. Aubert, P. B. Rand, C. Arnold, and R. L. Clough, Am. Chem. Soc. Preprints, Polymer Materials Science and Engineering, 57(2), 113(1987).

3. C. Arnold, J. H. Aubert, R. L. Clough, P. B. Rand, and A. P. Sylwester, U. S. Patent, 4,832,881, May 23, 1989.

4. D A. Schneider and R. A. Assink, Sandia Report SAND91-1591, 1991.

5. R. R. Lagasse, R. J. Weagley, P. K. Leslie, and D. A. Schneider, Am. Chem. Soc. Polymer Preprints, 32(1), 519 (1991).

6. K. Kamide et al., Polymer J., 17, 1233 (1985).

7. R. W. Vasofsky and J. D. Brown, Technical Report Y/DZ-692, Oak Ridge Y-12 Plant, Jan. 1990.

8. G. Henrici-Olive and S. Olive, Advances in Polymer Science, 32, 123 (1979).

9. G. Coppola et al., J. Appl. Polym. Sci, 16, 2829 (1972).

10. C. Azuma, Makromol. Chem., Makromol. Symp., 2, 169 (1986).

11. K. Kamide et al., Polymer J., 17, 607 (1985).

12. K. Kamide et al., Polymer J., 18, 819 (1986).

13. R. R. Lagasse, P. K. Leslie, C. Bero, and D. J. Plazek, Am. Chemical Society Symposium on Microcellular Materials, Washington, D.C., August 25, 1992 (to be published).

14. J. C. F. Wang, Org. 8431, "PAN Carbon Development Assessment," Memo to Distribution, May 29, 1990.

15. A. H. Compton and S. K. Allison, "X-rays in Theory and Experiment," Van Nostrand, Princeton, 1935.

16. W. D. Drotning, "Development of an Automated X-Ray Gauge for Nondestructive Quantitative Analysis," SAND88-0119, 1988.

17. B. Olivier, D. W. Schaefer, and R. R. Lagasse, unpublished results.

18. R. R. Lagasse, "Exceptionally Large Banded Spherulites," draft manuscript prepared for publication in Journal of Crystal Growth.

DISTRIBUTION:

1 Allied-Signal Aerospace Co.
Attn: H. M. Smith
Kansas City Division
P. O. Box 419159
Kansas City, MO 64141-6159

1 EG&G Mound Applied Technologies
Attn: R. J. DeSando, COS-3
P. O. Box 3000
Miamisburg, OH 45343-3000

1 Martin Marietta Energy Systems, Inc.
Attn: R. F. Simandl
Oak Ridge Y-12 Plant
Oak Ridge, TN 37831

1 Martin Marietta Energy Systems, Inc.
Attn: D. N. Robinson
Oak Ridge Y-12 Plant
Oak Ridge, TN 37831

1 1812 R. A. Assink Attn: D. A. Schneider
1 1815 J. H. Aubert
8 1815 R. R. Lagasse
1 1824 R. J. Weagley
1 2512 P. K. Leslie
1 2523 F. M. Delnick
1 2523 D. H. Doughty, Attn: N. Doddapaneni
1 2523 S. C. Levy
1 2752 K. R. Thompson, Attn: W. W. Shurtleff
1 6211 G. A. Carlson
1 6211 A. P. Sylwester
1 8347 A. E. Pontau
1 8600 L. A. West
1 8713 J. C. F. Wang
1 8716 W. R. Even
1 8716 M. C. Nichols
1 8523-2 Central Technical Files
5 7141 Technical Library
1 7151 Technical Publications
10 7613-2 Document Processing for DOE/OSTI

END

DATE FILMED

1/14/94